A closed-form analytical solution for thermal single-well injection-withdrawal tests

Yoojin Jung[1] and Karsten Pruess[1]

[1] Thermal single-well injection-withdrawal (SWIW) tests entail pumping cold water into a hot and usually fractured reservoir, and monitoring the temperature recovery during subsequent backflow. Such tests have been proposed as a potential means to characterize properties of enhanced geothermal systems (EGS), such as fracture spacing, connectivity, and porosity. In this paper we develop an analytical solution for thermal SWIW tests, using an idealized model of a single vertical fracture with linear flow geometry embedded in impermeable conductive wall rocks. The analytical solution shows that the time dependence of temperature recovery is dominated by the heat exchange between fracture and matrix rock, but strong thermal diffusivities of rocks as compared to typical solute diffusivities are not necessarily advantageous for characterizing fracture-matrix interactions. The effect of fracture aperture on temperature recovery during backflow is weak, particularly when the fracture aperture is smaller than 0.1 cm. The solution also shows that temperature recovery during backflow is independent of the applied injection and backflow rates. This surprising result implies that temperature recovery is independent of the height of the fracture, or the specific fracture-matrix interface areas per unit fracture length, suggesting that thermal SWIW tests will not be able to characterize fracture growth that may be achieved by stimulation treatments.

1. Introduction

[2] Enhanced geothermal systems (EGS) are engineered reservoirs that may be developed to produce energy from hot rock formations that are otherwise not economically viable for heat mining [Gérard et al., 2006]. To achieve a practically useful production capacity, the development of EGS commonly requires stimulation treatments, which usually involve water injection under high pressure. By applying stimulation treatments, we expect to increase the aperture, permeability, and size of pre-existing fractures and make additional fractures accessible to the injected fluid.

[3] While increased fracture permeability is advantageous for improving the production of thermal energy, rapid migration of the injected water through preferential paths with insufficient heat transfer from the rock may result in premature thermal breakthrough at production wells, which would reduce the lifetime of the geothermal reservoir. For both success and sustainability of EGS, it is critical to ascertain the effectiveness of stimulation treatments for enhancing the fracture-rock matrix interface area, reducing flow impedance in the reservoir, and increasing flow rates of production wells.

[4] Tracer tests have been proposed as a means to estimate fracture-matrix interface areas. Such tests generally involve the injection of aqueous solutes into one or more injection wells, and monitoring of tracer returns in fluids produced from offset observation or production wells [Shook, 2001; Sanjuan et al., 2006]. Interdiffusion of solute tracers between fractures and rock matrix produces characteristic tails in tracer breakthrough curves that may permit the determination of fracture-matrix interface areas [Pruess, 2002; Pruess et al., 2005; Shan and Pruess, 2005]. However, because tracer breakthrough at offset observation wells may be weak and slow, interwell tracer tests (ITT) may require fluid sampling over extended time periods of weeks or even months. Also, suitable observation wells may not always be available.

[5] Single-well injection-withdrawal (SWIW) tests, variously referred to as “huff and puff,” “push-pull,” or “injection-backflow” tests, can be an alternative to ITT. During an SWIW test, fluid with tracers is injected into a well and, after some quiescent or rest period, is produced out of the same well [Kocabas and Horne, 1987; Haggerty et al., 2001; Nalla and Shook, 2005; Ghergut et al., 2006, 2009; Neretnieks, 2007]. SWIW tests typically require a much shorter test duration from hours to a few days as compared to weeks or months for ITT. This holds out the promise of obtaining test results much more quickly, which would provide significant economic benefits. Another potential advantage is that SWIW tests are much less affected than ITT by heterogeneities in the fracture network, potentially providing a clearer signal of matrix properties

[1]Earth Sciences Division, Lawrence Berkeley National Laboratory, Berkeley, California, USA.

and fracture-matrix interaction parameters such as flow-wetted surface area (FWS), the all-important interface area between flowing fractures and wall rocks of low permeability [*Neretnieks and Moreno*, 2003; *Doughty and Tsang*, 2009]. The FWS is the critical parameter that determines achievable rates of rocks-to-fluid heat transfer, and thereby the productive capacity of the EGS reservoir.

[6] Past tests for estimating FWS have exclusively used solute tracers, but temperature itself may be used as a tracer [*Kocabas and Horne*, 1990; *Kocabas*, 2005, 2010; *Pruess and Doughty*, 2010]. Thermal SWIW tests would entail injecting cold water into a well and, after a certain quiescent or shut-in period, producing the water from the same well and monitoring the time dependence of temperature recovery. Using temperature as a tracer has potential advantages over reactive or nonreactive solute tracers for estimating heat transfer areas because temperature effects depend directly on the heat exchange between fracture and matrix, the essential process of heat mining that we aim to characterize; heat conduction is a diffusive process that is very "robust," depending as it does only on the thermal parameters of rocks and fluids, whereas solute diffusion is sensitive to tortuosity effects that may be difficult to characterize and add uncertainty to interpretation; thermal diffusivities of rocks are of order 10^{-6} m^2 s^{-1}, three orders of magnitude larger than typical solute diffusivities (four to five orders larger when considering tortuosity effects in rocks of low permeability), suggesting that effects of fracture-matrix exchange may be much stronger than for solute tracers; the local heat exchange between fluids and rocks is analogous to a reversible linear sorption of solute tracer, but the process depends only on robust thermal parameters, not on highly heterogeneous and difficult-to-characterize mineral abundances and surfaces as for sorbing solutes.

[7] Some research has been conducted to explore the utility of thermal SWIW tests. Analytical solutions for temperature return curves at the observation point (the well used for fluid injection and withdrawal) have been developed for a single fracture [*Kocabas and Horne*, 1990; *Kocabas*, 2005, 2010], and numerical simulations have shown possibilities for characterizing the properties of fractured reservoirs by thermal SWIW tests [*Pruess and Doughty*, 2010]. However, the earlier analytical solutions unfortunately include several typographical errors in their derivation process and final equations, and are limited to SWIW tests with no quiescent time. Because of the formulation methodology of the earlier solutions, developed only for the single observation point at the injection/withdrawal well, it would be impossible to extend the solution to include a finite rest period. On the other hand, numerical simulations for thermal SWIW tests are found to be very susceptible to space and time discretization errors. Therefore, a better approach is needed for a full understanding of the heat transport dynamics that affects the temperatures of the returning fluid during thermal SWIW tests.

[8] The objective of this study is to elucidate the potential of thermal SWIW tests for characterizing fractured reservoir properties. A theoretical approach is employed to understand the heat transport in a fractured rock under consideration of convective heat transfer within the fracture and conductive heat transfer in the adjacent rock matrix. We have developed an analytical solution for thermal SWIW tests in a fractured reservoir, and have applied this in a sensitivity analysis to evaluate the impact of fracture-matrix interface areas and effective fracture aperture on temperature recovery curves. Based on analytical studies, we discuss the possibilities and limitations for determining the thermal characteristics of fracture-matrix interactions by thermal SWIW tests. In addition, potential applications of our analytical solution are presented.

2. Theory

[9] We consider a vertically oriented fracture with uniform aperture $2b$ and porosity ϕ_f. The flow along the fracture is linear, and instantaneous thermal equilibrium is assumed for fluids and rocks within the fracture. The buoyancy flow in the vertical fracture is neglected. During the injection and withdrawal periods, it can be shown that viscous forces dominate buoyancy forces for the parameters of interest, and during the quiescent phase the temperature profile at the thermal front is diffuse, diminishing the tilting rate [*Hellström and Tsang*, 1988a, 1988b]. For simplicity, we further assume that conductive heat transport in the fracture is negligible, and consider heat conduction in the matrix only in the direction perpendicular to the fracture. The validity of this assumption is examined through numerical simulations, which indicate that this simplification has only a minor effect on return temperatures. Figure 1 shows a schematic of the conceptual model considered in this study. The x-axis is in the direction of the fracture, and the z-axis is perpendicular to the fracture-matrix interfaces. Because of symmetry, we need to consider only one-half of the actual model for the solution. The cold water is injected at a constant pore velocity, v, and after a finite quiescent time, the water is extracted from the injection well at the same pore velocity. During the quiescent period, v is assumed to

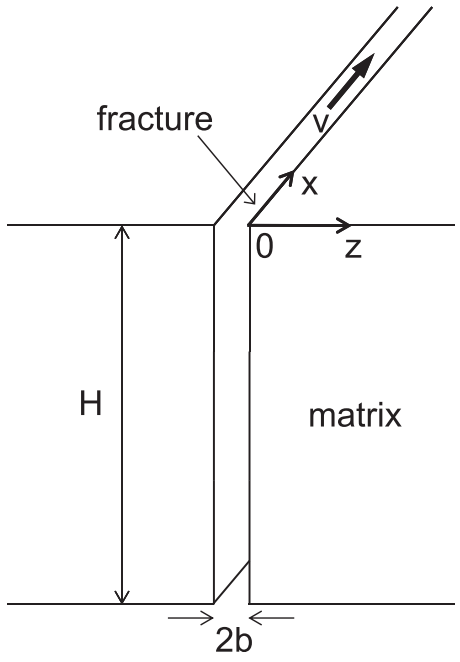

Figure 1. Perspective of a fracture with width $2b$, height H, and attached semi-infinite wall rocks.

be zero since v near a well quickly reaches steady state after the well is turned off [*Haggerty et al.*, 2001].

[10] With the assumptions above, the heat transport in the system during the injection phase can be described as follows (see "nomenclature" for notation):

$$\rho_f c_f \frac{\partial T_{f1}}{\partial t_1} + \rho_w c_w v \phi_f \frac{\partial T_{f1}}{\partial x} - \frac{k_m}{b} \frac{\partial T_{m1}}{\partial z}\bigg|_{z=0} = 0, \quad 0 \le x < \infty, \tag{1a}$$

$$\rho_m c_m \frac{\partial T_{m1}}{\partial t_1} - k_m \frac{\partial^2 T_{m1}}{\partial z^2} = 0, \quad 0 \le x < \infty, \ 0 \le z < \infty, \tag{1b}$$

where $\rho_f c_f = (1-\phi_f)\rho_m c_m + \phi_f \rho_w c_w$ is the specific heat of both rock and fluid in the fracture per unit volume, and pore velocity $v = q/(bH\phi_f)$ is constant along the fracture.

[11] We assume that the temperature is initially uniform throughout the system and the temperature of the injected fluid is constant during the injection phase. In addition, the temperature at the fracture walls is always the same as the temperature in the fracture. Then, the initial and boundary conditions can be expressed as

$$T_{f1} = T_{m1} = T_0 \quad \text{at} \quad t_1 = 0, \tag{2a}$$

$$T_{f1} = T_{inj} \quad \text{at} \quad x = 0, \tag{2b}$$

$$T_{f1} = T_{m1} \quad \text{at} \quad z = 0, \tag{2c}$$

$$T_{m1} \to T_0 \quad \text{as} \quad z \to \infty. \tag{2d}$$

[12] To simplify the analysis, we define the following dimensionless variables:

$$T_{f1D} = \frac{T_0 - T_{f1}}{T_0 - T_{inj}}; \quad T_{m1D} = \frac{T_0 - T_{m1}}{T_0 - T_{inj}}, \tag{3a}$$

$$x_D = \frac{k_m x}{\rho_w c_w v \phi_f b^2}; \quad z_D = \frac{z}{b}; \quad t_{1D} = \frac{k_m t_1}{\rho_f c_f b^2}, \tag{3b}$$

$$\theta = \frac{\rho_m c_m}{\rho_f c_f}. \tag{3c}$$

[13] Using the dimensionless variables, (1a) and (1b) can be rewritten:

$$\frac{\partial T_{f1D}}{\partial t_{1D}} + \frac{\partial T_{f1D}}{\partial x_D} - \frac{\partial T_{m1D}}{\partial z_D}\bigg|_{z_D=0} = 0 \tag{4a}$$

$$\theta \frac{\partial T_{m1D}}{\partial t_{1D}} - \frac{\partial^2 T_{m1D}}{\partial z_D^2} = 0 \tag{4b}$$

[14] The initial and boundary conditions become

$$T_{f1D} = T_{m1D} = 0 \quad \text{at} \quad t_{1D} = 0, \tag{5a}$$

$$T_{f1D} = 1 \quad \text{at} \quad x_D = 0, \tag{5b}$$

$$T_{f1D} = T_{m1D} \quad \text{at} \quad z_D = 0, \tag{5c}$$

$$T_{m1D} \to 0 \quad \text{as} \quad z_D \to \infty. \tag{5d}$$

Note that the dimensionless temperatures T_{f1D} and T_{m1D}, as defined in (3a), decrease from 1 to 0 as the original temperatures increase from the cold injection temperature T_{inj} to the hot initial rock temperature T_0. The reason for adopting this unusual convention is that it makes the initial conditions homogeneous as shown in (5a), which simplifies solution of the governing equations by Laplace transforms. The solution for this nonisothermal injection condition is available [*Lauwerier*, 1955]:

$$T_{f1D}(x_D, t_{1D}) = \operatorname{erfc} \frac{\sqrt{\theta} x_D}{2\sqrt{t_{1D} - x_D}} U(t_{1D} - x_D), \tag{6a}$$

$$T_{m1D}(x_D, z_D, t_{1D}) = \operatorname{erfc} \frac{\sqrt{\theta}(x_D + z_D)}{2\sqrt{t_{1D} - x_D}} U(t_{1D} - x_D), \tag{6b}$$

where U is the Heaviside step function:

$$U(y) = \begin{cases} 1 & \text{for } y > 0 \\ 0 & \text{for } y \le 0. \end{cases} \tag{7}$$

[15] During the quiescent period, the convective heat transfer in the fracture is neglected by the assumption of $v = 0$, simplifying the governing equations:

$$\frac{\partial T_{f2D}}{\partial t_{2D}} - \frac{\partial T_{m2D}}{\partial z_D}\bigg|_{z_D=0} = 0, \tag{8a}$$

$$\theta \frac{\partial T_{m2D}}{\partial t_{2D}} - \frac{\partial^2 T_{m2D}}{\partial z_D^2} = 0. \tag{8b}$$

Note that the time variable for the quiescent period is reassigned to distinguish it from that used for the injection phase, with the convention that $t_2 = 0$ at the beginning of the quiescent period. The dimensionless time variable for the quiescent phase t_{2D} is defined similar to t_{1D}, as shown in (3b).

[16] The temperature distribution at the end of injection is used as the initial condition for the quiescent period:

$$T_{f2D}(x_D, t_{2D} = 0) = T_{f1D}(x_D, t_{1D} = t_{Di}) = h_2(x_D), \tag{9a}$$

$$T_{m2D}(x_D, z_D, t_{2D} = 0) = T_{m1D}(x_D, z_D, t_{1D} = t_{Di}) = f_2(x_D, z_D), \tag{9b}$$

where t_{Di} is the dimensionless form of the total injection time t_i. The temperature at the rock matrix surface $z_D = 0$ is again assumed to be identical to the temperature in the fracture:

$$T_{f2D}(x_D, t_{2D}) = T_{m2D}(x_D, 0, t_{2D}) = g_2(x_D, t_{2D}). \tag{10}$$

[17] The equations (8a) and (8b) along with the constraints given by (9) and (10) are solved using the Laplace transformation. The detailed derivation process is shown in Appendix A, and the solutions for the quiescent period are shown below.

$$T_{f2D}(x_D,t_{2D}) = e^{\theta t_{2D}}\mathrm{erfc}(\sqrt{\theta t_{2D}}) \times T_{f2D}(x_D,t_{2D}=0) + \int_0^{t_{2D}} e^{\theta(t_{2D}-\tau)}\mathrm{erfc}(\sqrt{\theta[t_{2D}-\tau]}) \times \frac{\sqrt{\theta}}{2\sqrt{\pi\tau}}\int_0^{\infty} T_{m2D}(x_D,\eta,t_{2D}=0)\times\frac{\theta\eta}{\tau}e^{-\theta\eta^2/4\tau}\,\mathrm{d}\eta\,\mathrm{d}\tau, \tag{11a}$$

$$T_{m2D}(x_D,z_D,t_{2D}) = \frac{\sqrt{\theta}}{2\sqrt{\pi t_{2D}}}\int_0^{\infty} T_{m2D}(x_D,\eta,t_{2D}=0) \times \left[e^{-\theta(z_D-\eta)^2/4t_{2D}} - e^{-\theta(z_D+\eta)^2/4t_{2D}}\right]\mathrm{d}\eta + \int_0^{t_{2D}} T_{f2D}(x_D,\tau)\frac{\sqrt{\theta}z_D e^{-\theta z_D^2/4(t_{2D}-\tau)}}{2\sqrt{\pi}(t_{2D}-\tau)^{3/2}}\,\mathrm{d}\tau. \tag{11b}$$

[18] The governing equations for the withdrawal phase are similar to those for the injection phase. The only change is the negative sign for the convective heat transfer term due to the reversed flow direction during the withdrawal phase. In addition, t_3 is used as the time variable for the withdrawal phase, with the same convention that $t_3 = 0$ at the beginning of the withdrawal period. Therefore, the governing equations for the withdrawal phase in dimensionless form are

$$\frac{\partial T_{f3D}}{\partial t_{3D}} - \frac{\partial T_{f3D}}{\partial x_D} - \left.\frac{\partial T_{m3D}}{\partial z_D}\right|_{z_D=0} = 0, \tag{12a}$$

$$\theta\frac{\partial T_{m3D}}{\partial t_{3D}} - \frac{\partial^2 T_{m3D}}{\partial z_D^2} = 0, \tag{12b}$$

where $t_{3D} = k_m t_3/(\rho_f c_f b^2)$ is the dimensionless time variable for the withdrawal phase. The other dimensionless variables are identical to (3a)–(3c).

[19] The initial and boundary conditions are defined similar to those in the quiescent period. The temperature distribution at the end of the quiescent time is used as the initial condition for the withdrawal phase:

$$T_{f3D}(x_D,t_{3D}=0) = T_{f2D}(x_D,t_{2D}=t_{Dq}) = h_3(x_D), \tag{13a}$$

$$T_{m3D}(x_D,z_D,t_{3D}=0) = T_{m2D}(x_D,z_D,t_{2D}=t_{Dq}) = f_3(x_D,z_D), \tag{13b}$$

where t_{Dq} is the dimensionless form of the total quiescent time t_q. The temperature at the rock matrix surface $z_D = 0$ is,

$$T_{f3D}(x_D,t_{3D}) = T_{m3D}(x_D,0,t_{3D}) = g_3(x_D,t_{3D}). \tag{14}$$

[20] One important observation from the definition of the problem domain for the withdrawal phase is that the variation of fluid return temperatures with time will be independent of the flow rate. This surprising feature follows directly from the fact that, among the dimensionless variables used to describe the governing equations (12) and the initial and boundary conditions (13) and (14), the velocity term v only appears in the dimensionless distance x_D. Accordingly, the time dependence of temperature recovery at the injection/withdrawal well ($x = 0$) will be the same, regardless of the applied flow rate. This novel result has important ramifications for the feasibility of thermal SWIW tests, which will be discussed in more depth in the Results and Discussion section (section 3), below.

[21] The detailed derivation process is given in Appendix B, and the analytical solution for the withdrawal phase is found to be

$$T_{f3D}(x_D,t_{3D}) = \int_0^{\min(t_{3D},t_{Dq}-x_D)}\frac{\sqrt{\theta}\xi}{2}\frac{e^{-\theta\xi^2/4(t_{3D}-\xi)}}{\sqrt{\pi(t_{3D}-\xi)^3}} \times T_{f3D}(x_D+\xi,0)\,\mathrm{d}\xi + \int_0^{t_{3D}}\int_0^{\min(\tau,t_{Dq}-x_D)}\frac{\sqrt{\theta}\xi}{2}\frac{e^{-\theta\xi^2/4(\tau-\xi)}}{\sqrt{\pi(\tau-\xi)^3}} \times\theta\int_0^{\infty} T_{m3D}(x_D+\xi,\eta,0)\times\frac{\sqrt{\theta}\eta}{2} \times\frac{e^{-\theta\eta^2/4[t_{3D}-\tau]}}{\sqrt{\pi(t_{3D}-\tau)^3}}\,\mathrm{d}\eta\,\mathrm{d}\xi\,\mathrm{d}\tau. \tag{15}$$

Note here that the final solution (15) includes the given initial condition at the beginning of the withdrawal phase for both fracture and matrix. Therefore, when a SWIW test is conducted with no quiescent time, the temperature distribution at the end of the injection phase becomes the initial condition of the withdrawal phase, and the solution (15) can simply be rewritten as

$$T_{f3D}(x_D,t_{3D}) = \int_0^{\min(t_{3D},t_{Di}-x_D)}\frac{\sqrt{\theta}\xi}{2}\frac{e^{-\theta\xi^2/4[t_{3D}-\xi]}}{\sqrt{\pi(t_{3D}-\xi)^3}} \times T_{f1D}(x_D+\xi,t_{Di})\,\mathrm{d}\xi + \int_0^{t_{3D}}\int_0^{\min(\tau,t_{Di}-x_D)}\frac{\sqrt{\theta}\xi}{2}\frac{e^{-\theta\xi^2/4(\tau-\xi)}}{\sqrt{\pi(\tau-\xi)^3}} \times\theta\int_0^{\infty} T_{m1D}(x_D+\xi,\eta,t_{Di})\times\frac{\sqrt{\theta}\eta}{2} \times\frac{e^{-\theta\eta^2/4[t_{3D}-\tau]}}{\sqrt{\pi(t_{3D}-\tau)^3}}\,\mathrm{d}\eta\,\mathrm{d}\xi\,\mathrm{d}\tau, \tag{16}$$

with the convention that $t_3 = 0$ at the beginning of the withdrawal period.

3. Results and Discussion

3.1. Verification of Solution

[22] Although the analytical solutions (15) and (16) have the identical form, different methods are used for calculation due to the difference in the initial conditions at the beginning of the withdrawal period. If writing out all of the terms in (15), the analytical solution (15) for SWIW tests involving injection, quiescent, and withdrawal phases includes a six-dimensional improper integral. The integrand goes to a finite limiting value at finite upper and lower limits, but cannot be evaluated on at least one of those limits because of an integrable singularity at the limit, and some of the upper limits are infinite. In addition, variable upper limits of the integration make the numerical calculation of the integral more complicated. To obtain accurate results, the solution (15) is calculated using a numerical integration technique based on the extended midpoint rule in combination with recursive adaptive algorithms. On the other hand, the solution (16), which is for SWIW tests with no quiescent period, is simply computed using Mathcad (Parametric Technology Corporation, Needham, MA) since it requires numerical integration only in two and three dimensions.

[23] In order to verify the analytical solutions (15) and (16), the equations are compared with numerical solutions using TOUGH2 [*Pruess et al.*, 1999]. TOUGH2 is a numerical code for nonisothermal flows of multiphase, multicomponent fluids, and has been widely verified against many analytical solutions. The parameter values used for comparison are listed in Table 1. The grid for the fracture consists of 1000 blocks of 1 cm thickness each, for a total length of 10 m in the x direction. The matrix domain is discretized in a nonuniform way to accurately model the heat exchange between the fracture and the rock matrix; the grid spacing for the matrix gradually increases from 0.01 cm at the fracture wall to 2 m, for a total length of 10 m in the z direction, so as to be infinite-acting for the time period considered here. At the end of the fracture opposite the injection block, boundary conditions are maintained constant at their initial values. The analytical solutions show excellent agreement with the TOUGH2 simulations for $t_q = 0$ h and $t_q = 5$ h (see Figure 2). At the beginning of the withdrawal period, the fluid temperature for $t_q = 5$ h is ~82°C higher than that for $t_q = 0$ h, indicating that conductive heat transfer from the rock matrix produces significant changes in the temperature returns. Note that TOUGH2 normally updates the specific heat and density of water at every time step according to the change in temperature. Here this functionality in TOUGH2 was turned off to compare with the analytical solution, which assumes these parameters to be constant throughout the system over time.

Table 1. Parameter Values Used for TOUGH2 Simulation

Reservoir Properties	Value
Fracture permeability	5×10^{-12} m^2
Matrix permeability	1×10^{-18} m^2
Fracture porosity, ϕ_f	0.5
Fracture aperture, $2b$	2 cm
Fracture height, H	50 m
Thermal conductivity of matrix, k_m	2.1 W/m/°C
Specific heat of matrix, c_m	1000 J/kg/°C
Density of matrix, ρ_m	2650 kg m^{-3}
Injection/withdrawal pore velocity, v	4×10^{-4} m s^{-1}
Temperature of injected water, T_{inj}	20°C
Total injection time, t_i	5 h
Total quiescent time, t_q	0 or 5 h
Specific heat of water, c_w	4200 J/kg/°C
Density of water, ρ_w	1000 kg m^{-3}
Initial conditions	
Pressure	200 bar
Temperature, T_0	200°C

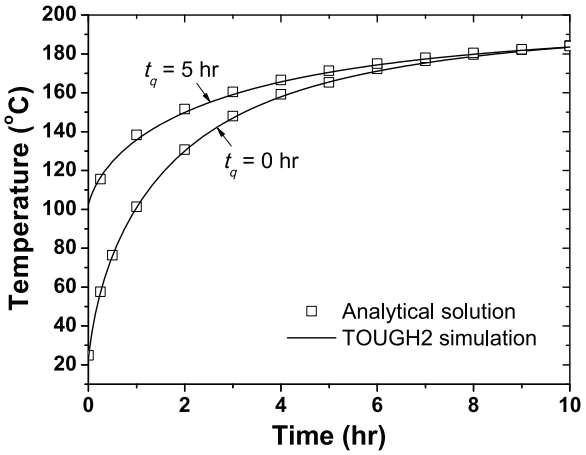

Figure 2. Comparison of the analytical solution with the numerical (TOUGH2) solution for $t_q = 0$ h and $t_q = 5$ h. Temperature return profiles at $x = 0$ during the withdrawal period.

[24] While the results are found to be sufficiently accurate for solutions (15) and (16), the difference in computational effort between two cases is substantial. For the case of no quiescent time, the analytical solution evaluation is much faster than TOUGH2 (<10 min versus several hours), but with a rest period, TOUGH2 becomes much faster than the analytical solution evaluation. The solution (15) converges extremely slowly, and it takes up to 1 week for computing one point shown in Figure 2. Determining how this type of multidimensional improper integral is best handled is a nontrivial problem. Seeking an efficient solution scheme, while truly worthwhile, will require significant effort, and is considered beyond the scope of this study. Therefore, the focus of sensitivity analysis will be on SWIW tests with no quiescent period.

3.2. Sensitivity Analysis

[25] The analytical solution developed for thermal SWIW tests can be a useful tool for estimating system parameters and sensitivities relevant to the heat exchange between fracture and matrix rock. In order to obtain reasonable estimates and avoid misinterpretation of data, it is important to assess the sensitivity of temperature recovery to the various parameters of interest.

[26] From the analytical solution (16), we can infer that at the injection/withdrawal well ($x = 0$), t_{Di} and θ are the only parameters affecting temperature return curves. According to (3b) and (3c), since the thermal parameters (ρ, c, k) of rocks and fluids can be assumed to be constant

during a SWIW test and may be assumed to be known, t_{Di} and θ are dependent on only b, ϕ_f, and t_i. Therefore, sensitivity analysis is conducted for these key parameters. Unless otherwise indicated, the parameters in Table 1 are used as the reference conditions to calculate temperature return curves at $x = 0$, and only one parameter at a time is varied.

[27] Figure 3 shows the effect of fracture half-aperture b on the return temperatures. As the fracture aperture increases, the temperature recovery becomes slower. However, the differences between temperature-return curves become smaller when b decreases, and the curves converge to one another when b is smaller than 0.1 cm. That is, when the fracture aperture is sufficiently small compared to the available heat transfer area between the fracture and rock matrix, the heat conduction from the matrix is a predominant mechanism controlling the temperature change within the fracture. This can be further supported by our analytical solution. As shown in the Fourier-Laplace space solution (B6) and the real space solution (16), the return temperatures are determined by the integrated effects of the initial temperature within the fracture and the heat flux at the fracture-matrix interfaces over time and space. Figure 4 shows the fraction of thermal energy in the produced fluid (relative to injection temperature) that is contributed by conductive heat transfer from the adjacent rock matrix. The fraction rapidly increases within the first 1 h, and reaches up to 0.99 for fracture half-apertures $b \leq 0.1$ cm, thereby explaining the insensitivity of the temperature return curves to b in this range in Figure 3.

[28] The temperature return curves are insensitive to ϕ_f (see Figure 5). At $x = 0$, ϕ_f only appears in $\rho_f c_f = (1 - \phi_f)\rho_m c_m + \phi_f \rho_w c_w$. Based on the values in Table 1, $\rho_m c_m$ and $\rho_w c_w$ have comparable magnitude of $\sim 4.2 \times 10^6$ and 2.65×10^6 J/m^3/°C, respectively, so that $\rho_f c_f$ depends only weakly on ϕ_f. As a result, the change of ϕ_f has a minor impact on the temperature return curves. Note that even if temperatures are measured at locations other than $x = 0$, return temperatures are not sensitive to ϕ_f. As shown in (3b), ϕ_f in the dimensionless parameter x_D is cancelled out by the velocity term v, which for a fixed injection/production rate $q = vbH\phi_f$ is inversely proportional to ϕ_f.

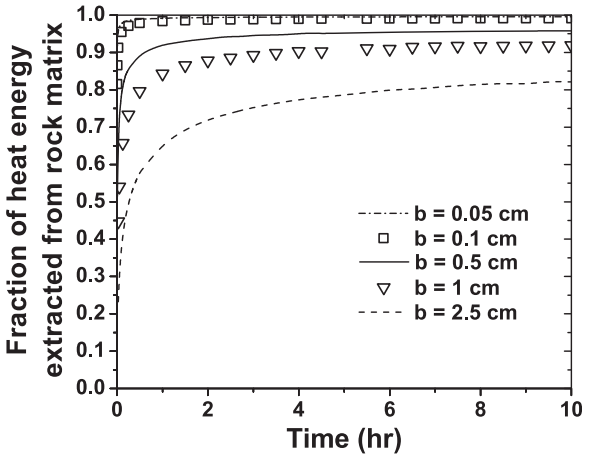

Figure 4. Effect of b (half-fracture aperture) on the fraction of heat energy extracted from the rock matrix.

[29] Figures 6a and 6b show the temperature return curves for different injection times of $t_i = 1$ h and $t_i = 10$ h, respectively. As the injection time is reduced, the differences between the temperature-return profiles for different b become more distinct. At the same time, however, the range of investigation is reduced (see Figure 7), making the estimated parameters less significant because the region characterized by the test is becoming too small to represent the fractured rock of interest. Note that among the parameters involved in t_{Di}, injection time t_i is the only factor that can actually be controlled to improve the sensitivity of SWIW tests.

[30] As had been mentioned above, temperature recovery is independent of the applied injection/withdrawal flow velocity v. This insensitivity is a consequence of the dimensionless parameters admitted by the problem, and does not depend on the detailed form of the analytical solution (16). It precludes determining fracture height, or an increase thereof achieved by stimulation treatments, from a thermal SWIW test.

[31] It is remarkable that the flow rate has no influence on the return temperatures at the observation point ($x = 0$).

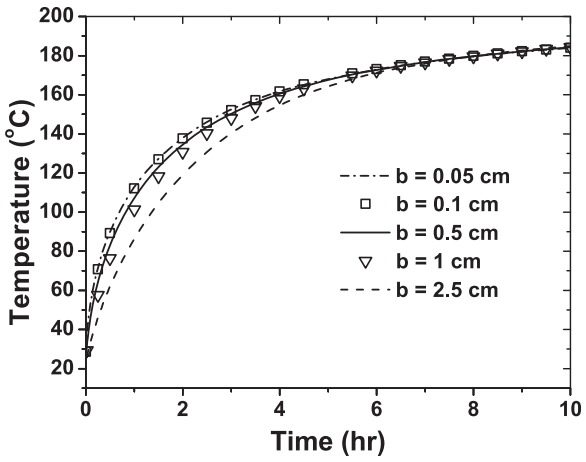

Figure 3. Effect of b (half-fracture aperture) on temperature return profiles.

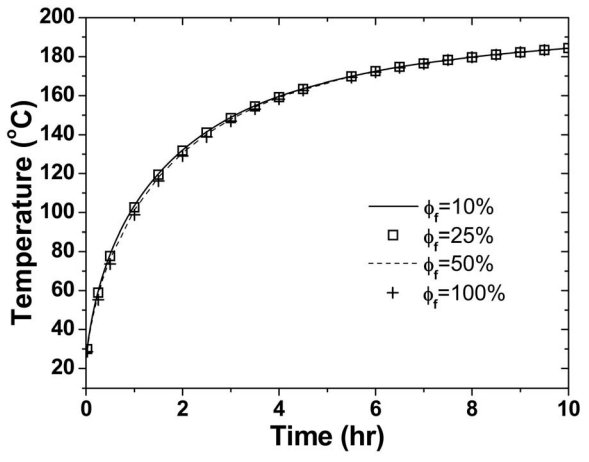

Figure 5. Effect of ϕ_f (porosity of fracture) on temperature return profiles.

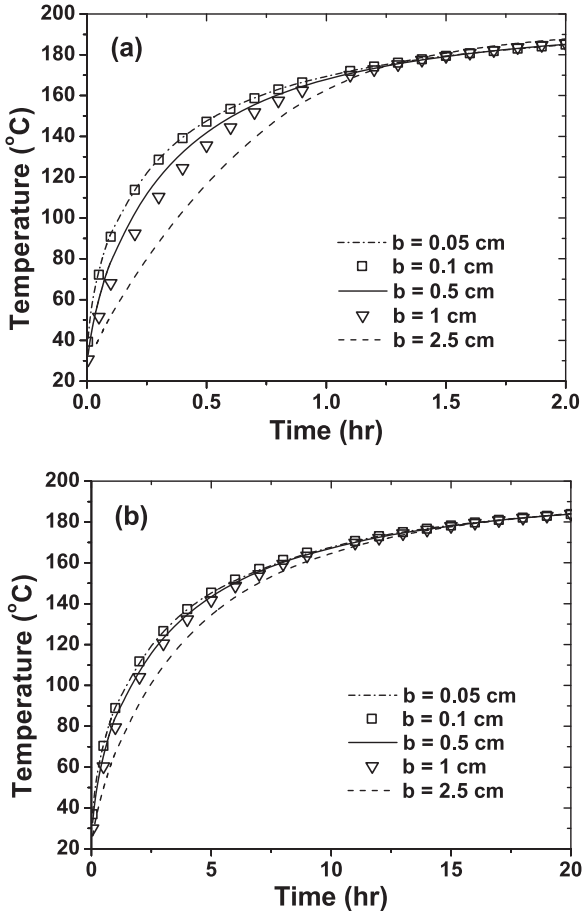

Figure 6. Effect of b (half fracture aperture) on temperature return profiles (a) for $t_i = 1$ h and (b) for $t_i = 10$ h.

The sensitivity of return temperatures to changes in flow velocity, $\partial T_{f3D}/\partial v$, increases approximately linearly with distance x from the fracture inlet, and converges to zero as the injection/withdrawal well is approached (Figure 8).

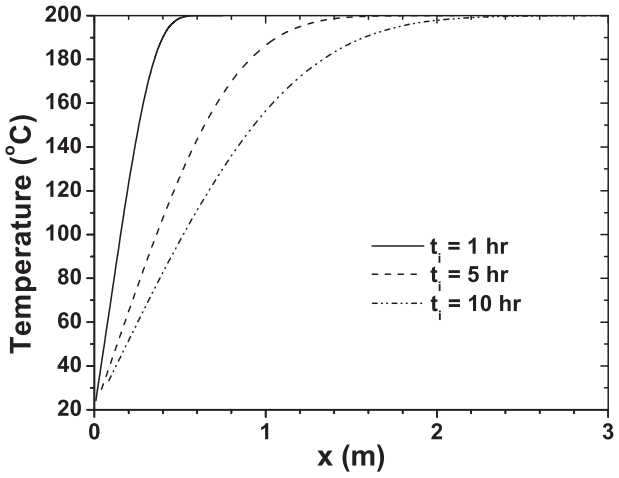

Figure 7. Spatial profiles of temperature in the fracture after injection at a pore velocity of 4×10^{-4} m s^{-1} for time periods of 1, 5, and 10 h.

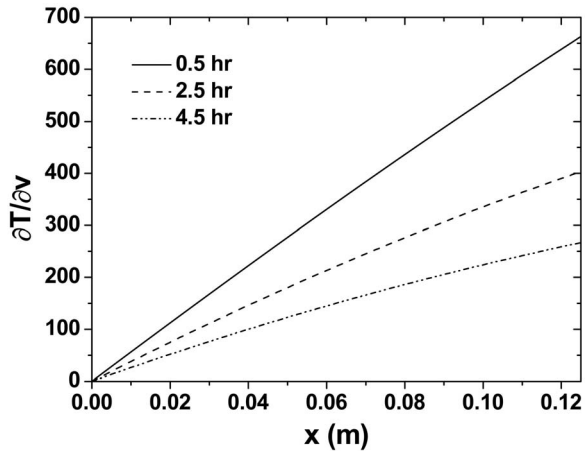

Figure 8. Variations of $\partial T_{f3D}/\partial v$ as a function of x at $t_3 = 0.5$, 2.5, and 4.5 h after the beginning of the withdrawal period.

This means that the time dependence of temperature recovery at $x = 0$ will be identical regardless of the flow rate. A change of flow rate affects both the cooling rate during the injection period and the reheating rate during the withdrawal period, but the effects are remarkably compensated at $x = 0$.

[32] Among the most important changes in EGS reservoirs sought and expected from stimulation treatments are increasing the fracture height (equal to fracture-matrix interface areas per unit length), and establishing connectivity for and gaining access to additional fractures. Both of these effects would increase the area available for heat transfer to the injected fluid and improve the rate of heat extraction from the reservoir rock. For a fixed injection/withdrawal rate, either change will reduce the flow velocity in the fractures which, as seen from our analytical solution, has no effect on temperature recovery at the injection/withdrawal location $x = 0$. The insensitivity of temperature recovery to applied flow rate at $x = 0$ implies that thermal SWIW tests are not able to characterize the specific fracture-matrix interface area, which is the reservoir parameter of greatest interest for long-term heat mining.

[33] The insensitivity of thermal SWIW tests to the injection/withdrawal flow velocity, on the other hand, is ideal for evaluating the thermal diffusivity of the rock matrix, because the influence of advective heterogeneity can be disregarded. More importantly, this independence on the flow velocity also holds for SWIW tests using solute tracers because local heat exchange between fluids and rocks is analogous to reversible linear sorption of solute tracers. While the thermal diffusivity of a rock matrix is commonly assumed to be known for EGS reservoirs, diffusion and sorption properties of solute tracers, including contaminants such as radionuclides and chemical wastes, are important parameters that have to be measured through field tests [*Haggerty et al.*, 2001; *Moreno et al.*, 1997; *Neretnieks*, 2007; *Schroth et al.*, 2001]. Therefore, the analytical solution developed for thermal SWIW tests can be applied for analyzing SWIW tests using solute tracers and evaluating in situ diffusion and sorption coefficients of solute tracers.

3.3. Application

[34] As the transform of the initial condition is inverted back to the original form by the convolution theorem (see Appendices A and B), the initial condition is not solved to find the transform during the derivation process. Accordingly, the final solutions (15) and (16) include the given initial condition for both fracture and matrix. The advantage of this approach is that different initial conditions can easily be applied to our analytical solution. As an example, we show here the application to a thermal SWIW test with slug-like cold-water injection, in which cold water is injected for a limited time period, after which injection continues at the original reservoir temperature T_0. For this case, the boundary condition at the fracture inlet $x_D = 0$ can be written:

$$T_{f1D} = 1 - U(t_{1D} - t_{Ds}) = \begin{cases} 1 & \text{for} \quad 0 \le t_{1D} \le t_{Ds} \\ 0 & \text{for} \quad t_{1D} > t_{Ds}, \end{cases} \tag{17}$$

where t_{Ds} is the dimensionless form of the tracer injection time t_s, and should be smaller than t_{Di}.

[35] By linearity, the solution for this slug injection test can be derived from the solution for the step injection test shown in (6). The temperature distribution at the end of the injection and the beginning of the withdrawal period is

$$T_{f1D}(x_D, t_{Di}) = T_{f3D}(x_D, t_{2D} = 0) = \operatorname{erfc}\frac{\sqrt{\theta}x_D}{2\sqrt{t_{Di} - x_D}} U(t_{Di} - x_D) - \operatorname{erfc}\frac{\sqrt{\theta}x_D}{2\sqrt{t_{Di} - t_{Ds} - x_D}} U(t_{Di} - t_{Ds} - x_D), \tag{18a}$$

$$T_{m1D}(x_D, z_D, t_{Di}) = T_{m3D}(x_D, z_D, t_{2D} = 0) = \operatorname{erfc}\frac{\sqrt{\theta}(x_D + z_D)}{2\sqrt{t_{Di} - x_D}} U(t_{Di} - x_D) - \operatorname{erfc}\frac{\sqrt{\theta}(x_D + z_D)}{2\sqrt{t_{Di} - t_{Ds} - x_D}} U(t_{Di} - t_{Ds} - x_D). \tag{18b}$$

Substituting (18) into (16) gives the solution for the SWIW test with a slug-like cold water injection.

[36] Because of a mathematical equivalence between reversible linear sorption and local heat exchange between fluids and rocks [*Pruess et al.*, 2005], the analytical solution for slug-like nonisothermal injection can also be applied to SWIW tests using solute tracers, which commonly use slug-like tracer injection. However, because typical solute diffusivities are three orders of magnitude smaller than thermal diffusivities of rocks (equal to $k_m/\rho_m c_m$), a much weaker fracture-matrix interaction is expected when solute tracers are used. Figure 9 shows the difference between the breakthrough curve for a solute tracer and the temperature return curve; the peak of the breakthrough curve for the solute tracer is substantially higher than that of the temperature return curve. Here the diffusivity of the solute tracer is smaller than the thermal diffusivity of the rock matrix by a factor of 10^3, and the parameters shown in Table 1 are used except $t_s = 5$ h and $t_i = 10$ h. The match with the TOUGH2 simulations is again excellent, showing the robustness of our analytical solution. It should be noted that the dimensionless concentrations increase from 0 to 1 as the solute concentrations increase from the initial background concentration to the injection concentration, unlike the dimensionless temperatures.

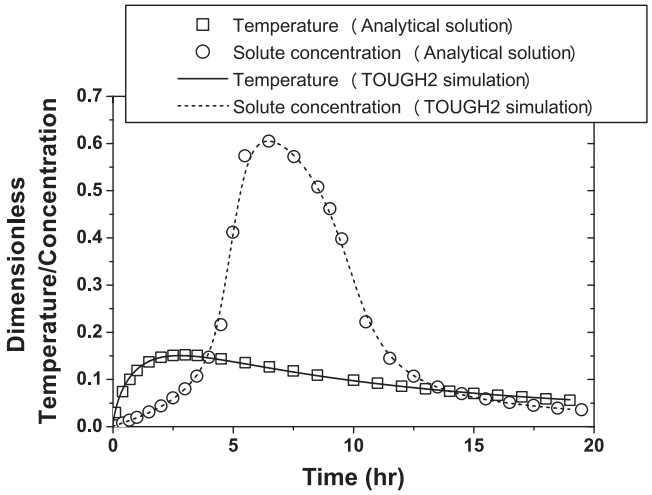

Figure 9. Comparison of the breakthrough curve for a typical solute tracer with the temperature return curve.

[37] The superposition concept used in this example can be generalized to treat any time series of tracer injection steps. Therefore, with our novel approach of handling the initial condition throughout the derivation procedure, our analytical solution can theoretically be extended for "nonideal" SWIW tests, where the injection and withdrawal rates have step changes with any number of intermittent quiescent periods. The condition at the end of each previous step becomes the initial condition for the current step, and the solution for each step can be derived using the procedure shown either in Appendix A for a quiescent period or in Appendix B for a withdrawal period. In this way, the solution with a nested structure will be developed. This suggests that the validity of flow velocity independence remains intact for nonideal SWIW tests. While it is straightforward to derive an analytical solution for nonideal SWIW tests, the practical utility of the analytical solution is yet limited due to the difficulty in evaluating the solution with present techniques.

4. Concluding Remarks

[38] An analytical solution has been developed to explore the possibilities of thermal SWIW tests for characterizing fractured reservoir properties, particularly related to fracture-matrix interactions. While direct application of the analytical solution may not be possible for most practical cases due to the simplified geometric conditions in our model, the analytical solution reveals some unexpected but important results that are of great value for understanding the fundamentals of heat transfer in fractured reservoirs. Temperature return curves do depend on fracture aperture,

but the sensitivity of temperature returns to the fracture aperture is not large. For the single fracture considered in this study, heat transfer from the rock matrix is rapid and overwhelming for practically relevant fracture apertures. The differences in the temperature return curves for different fracture apertures may not be distinct enough to determine the parameter value. Our analysis also shows that the return temperatures are insensitive to flow rate. This remarkable and novel result, not achieved in previous work, implies that changes in fracture-matrix interface areas due to reservoir stimulation do not provide an observable signal in thermal SWIW tests.

Appendix A: Derivation of Analytical Solution for Quiescent Period

[39] By superposition, the solution to (8b) satisfies the following:

$$T_{m2D} = T_{m2D,1} + T_{m2D,2}, \tag{A1}$$

where $T_{m2D,1}$ and $T_{m2D,2}$ are solutions of the two problems

$$\theta\frac{\partial T_{m2D,1}}{\partial t_{2D}} - \frac{\partial^2 T_{m2D,1}}{\partial z_D^2} = 0, \tag{A2a}$$

$$T_{m2D,1}(x_D, 0, t_{2D}) = 0 \quad (0 < t_{2D} < \infty), \tag{A2b}$$

$$T_{m2D,1}(x_D, z_D, 0) = \operatorname{erfc}\frac{\sqrt{\theta}(x_D + z_D)}{2\sqrt{t_{Di} - x_D}}U(t_{Di} - x_D) = f_2(x_D, z_D) \quad (0 \le z_D < \infty), \tag{A2c}$$

and

$$\theta\frac{\partial T_{m2D,2}}{\partial t_{2D}} - \frac{\partial^2 T_{m2D,2}}{\partial z_D^2} = 0, \tag{A3a}$$

$$T_{m2D,2}(x_D, 0, t_{2D}) = T_{f2D}(x_D, t_{2D}) = g_2(x_D, t_{2D}) \quad (0 \le t_{2D} < \infty), \tag{A3b}$$

$$T_{m2D,2}(x_D, z_D, 0) = 0 \quad (0 < z_D < \infty). \tag{A3c}$$

[40] First, the solution to (A2) is obtained using the method of images; the problem domain is extended to $z_D = -\infty$. Calling the extended function $f_{2,\text{ext}}$, we choose $f_{2,\text{ext}}$ to be the odd extension of $f_2(x_D, z_D)$, which automatically satisfies the boundary condition (A2b). Then, applying the Fourier transform to (A2a) with respect to z_D, we obtain

$$\frac{1}{\theta}(i\omega)^2\hat{T}_{m2D,1} = \frac{\partial \hat{T}_{m2D,1}}{\partial t_{2D}}, \tag{A4}$$

where $\hat{T}$ is the temperature in the Fourier space. The general solution for (A4) is

$$\hat{T}_{m2D,1} = Ae^{-\frac{1}{\theta}\omega^2 t_{2D}}, \tag{A5}$$

where A is constant. Applying the Fourier transformed boundary condition of (A2c), we obtain

$$A = \hat{f}_{2,\text{ext}}(x_D, \omega). \tag{A6}$$

Substituting (A6) to (A5) and then using ωωthe Fourier convolution principle, the solution for (A2) is

$$\begin{aligned} T_{m2D,1}(x_D, z_D, t_{2D}) &= f_{2,\text{ext}}(x_D, z_D) * \frac{\sqrt{\theta}}{2\sqrt{\pi t_{2D}}}e^{-\theta z_D^2/4t_{2D}} \\ &= \frac{\sqrt{\theta}}{2\sqrt{\pi t_{2D}}}\int_{-\infty}^{\infty} f_{2,\text{ext}}(x_D, \eta)e^{-\theta(z_D-\eta)^2/4t_{2D}}\,\mathrm{d}\eta \\ &= \frac{\sqrt{\theta}}{2\sqrt{\pi t_{2D}}}\int_0^{\infty} f_2(x_D, \eta)[e^{-\theta(z_D-\eta)^2/4t_{2D}} - e^{-\theta(z_D+\eta)^2/4t_{2D}}]\,\mathrm{d}\eta. \end{aligned} \tag{A7}$$

As shown in (A7), the solution is expressed only over the actual domain, $0 \le z_D < \infty$, and the fictitious extension is eliminated.

[41] Next, applying the Laplace transform with respect to t_{2D}, (A3a) becomes

$$\frac{1}{\theta}\frac{\partial^2 \overline{T}_{m2D,2}}{\partial z_D^2} = s\overline{T}_{m2D,2}, \tag{A8}$$

where $\overline{T}$ is the temperature in the Laplace space. The general solution for (A8) is

$$\overline{T}_{m2D,2} = Be^{-\sqrt{s\theta}z_D}, \tag{A9}$$

where B is constant. Applying the boundary condition (A3b), we obtain

$$B = \overline{g}_2(x_D, s). \tag{A10}$$

Substituting (A10) for (A9) and using the Laplace convolution theorem, the solution for (A3) is

$$\begin{aligned} T_{m2D,2}(x_D, z_D, t_{2D}) &= g_2(x_D, t_{2D}) * \frac{\sqrt{\theta}z_D e^{-\theta z_D^2/4t_{2D}}}{2\sqrt{\pi}t_{2D}^{3/2}} \\ &= \int_0^{t_{2D}} g_2(x_D, \tau)\frac{\sqrt{\theta}z_D e^{-\theta z_D^2/4(t_{2D}-\tau)}}{2\sqrt{\pi}(t_{2D}-\tau)^{3/2}}\,\mathrm{d}\tau. \end{aligned} \tag{A11}$$

By approximation to the identity [*Folland*, 1995], since $g_2(x_D, t_{2D})$ is continuous on R^n with support in $[0,\infty) \times [0,\infty)$, $T_{m2D,2}(x_D, z_D, t_{2D})$ converges uniformly to $g_2(x_D, t_{2D})$ as $z_D \to 0$, meaning that $T_{m2D,2}(x_D, z_D, t_{2D})$ is continuous on $[0,\infty) \times [0,\infty) \times [0,\infty)$ with $T_{m2D,2}(x_D, 0, t_{2D}) = g_2(x_D, t_{2D})$. Similarly, $T_{m2D,1}(x_D, z_D, t_{2D})$ in (A7) satisfies the initial condition (A2c).

[42] From (A1) therefore, the solution of (8b) is

$$\begin{aligned} T_{m2D}(x_D, z_D, t_{2D}) = \frac{\sqrt{\theta}}{2\sqrt{\pi t_{2D}}}&\int_0^{\infty} f_2(x_D, \eta) \\ &\times [e^{-\theta(z_D-\eta)^2/4t_{2D}} - e^{-\theta(z_D+\eta)^2/4t_{2D}}]\,\mathrm{d}\eta \\ &+ \int_0^{t_{2D}} g_2(x_D, \tau)\frac{\sqrt{\theta}z_D e^{-\theta z_D^2/4(t_{2D}-\tau)}}{2\sqrt{\pi}(t_{2D}-\tau)^{3/2}}\,\mathrm{d}\tau. \end{aligned} \tag{A12}$$

[43] Applying the Laplace transform to (8a) with respect to t_{2D}, we obtain

$$s\overline{T}_{f2D} - T_{f2D}(x_D,0) - \left.\frac{\partial \overline{T}_{m2D}}{\partial z_D}\right|_{z_D=0} = 0. \tag{A13}$$

From (A1) and (A11),

$$\left.\frac{\partial \overline{T}_{m2D}}{\partial z_D}\right|_{z_D=0} = \left.\frac{\partial \overline{T}_{m2D,1}}{\partial z_D}\right|_{z_D=0} - \sqrt{s\theta}\,\overline{g}_2(x_D,s). \tag{A14}$$

Substituting (A14) for (A13) and then rewriting (A13),

$$(s+\sqrt{s\theta})\overline{T}_{f2D} - h_2(x_D) - \left.\frac{\partial \overline{T}_{m2D,1}}{\partial z_D}\right|_{z_D=0} = 0. \tag{A15}$$

Then,

$$\overline{T}_{f2D} = \frac{1}{s+\sqrt{s\theta}}\left[h_2(x_D) + \left.\frac{\partial \overline{T}_{m2D,1}}{\partial z_D}\right|_{z_D=0}\right]. \tag{A16}$$

By applying the inverse Laplace transform and using the Laplace convolution principle,

$$\begin{aligned} T_{f2D} = {} & e^{\theta t_{2D}}\mathrm{erfc}(\sqrt{\theta t_{2D}}) \times h_2(x_D) \\ & + \int_0^{t_{2D}} e^{\theta(t_{2D}-\tau)}\mathrm{erfc}(\sqrt{\theta[t_{2D}-\tau]}) \times \left.\frac{\partial T_{m2D,1}}{\partial z_D}\right|_{z_D=0} \mathrm{d}\tau. \end{aligned} \tag{A17}$$

From (A7),

$$\left.\frac{\partial T_{m2D,1}}{\partial z_D}\right|_{z_D=0} = \frac{\sqrt{\theta}}{2\sqrt{\pi t_{2D}}}\int_0^{\infty} f_2(x_D,\eta)\frac{\theta\eta}{t_{2D}} e^{-\theta\eta^2/4t_{2D}}\,\mathrm{d}\eta. \tag{A18}$$

Therefore, substituting (A18) and the initial condition (9) into (A17) yields the solution for the fracture temperature in the real domain during the quiescent period:

$$\begin{aligned} T_{f2D}(x_D,t_{2D}) = {} & e^{\theta t_{2D}}\mathrm{erfc}(\sqrt{\theta t_{2D}}) \times T_{f2D}(x_D,t_{2D}=0) \\ & + \int_0^{t_{2D}} e^{\theta(t_{2D}-\tau)}\mathrm{erfc}(\sqrt{\theta[t_{2D}-\tau]}) \\ & \times \frac{\sqrt{\theta}}{2\sqrt{\pi\tau}}\int_0^{\infty} T_{m2D}(x_D,\eta,t_{2D}=0) \\ & \times \frac{\theta\eta}{\tau} e^{-\theta\eta^2/4\tau}\mathrm{d}\eta\,\mathrm{d}\tau. \end{aligned} \tag{A19}$$

The solution for the matrix temperature during the quiescent period is obtained from (9b), (10), and (A12):

$$\begin{aligned} T_{m2D}(x_D,z_D,t_{2D}) = {} & \frac{\sqrt{\theta}}{2\sqrt{\pi t_{2D}}}\int_0^{\infty} T_{m2D}(x_D,\eta,t_{2D}=0) \\ & \times \left[e^{-\theta(z_D-\eta)^2/4t_{2D}} - e^{-\theta(z_D+\eta)^2/4t_{2D}}\right]\mathrm{d}\eta \\ & + \int_0^{t_{2D}} T_{f2D}(x_D,\tau)\frac{\sqrt{\theta}z_D e^{-\theta z_D^2/4(t_{2D}-\tau)}}{2\sqrt{\pi}(t_{2D}-\tau)^{3/2}}\,\mathrm{d}\tau. \end{aligned} \tag{A20}$$

Appendix B: Derivation of Analytical Solution for Withdrawal Period

[44] The derivation procedure of T_{m3D} is identical to that of T_{m2D} described in Appendix A, and therefore the solution of (12b) is

$$\begin{aligned} T_{m3D}(x_D,z_D,t_{3D}) = {} & \frac{\sqrt{\theta}}{2\sqrt{\pi t_{3D}}}\int_0^{\infty} f_3(x_D,\eta)\left[e^{-\theta(z_D-\eta)^2/4t_{3D}}\right. \\ & \left. - e^{-\theta(z_D+\eta)^2/4t_{3D}}\right]\mathrm{d}\eta \\ & + \int_0^{t_{3D}} g_3(x_D,\tau)\frac{\sqrt{\theta}z_D e^{-\theta z_D^2/4(t_{3D}-\tau)}}{2\sqrt{\pi}(t_{3D}-\tau)^{3/2}}\,\mathrm{d}\tau. \end{aligned} \tag{B1}$$

[45] Then, applying the Laplace transform to (12a) with respect to t_{3D}, we obtain

$$s\overline{T}_{f3D} - T_{f3D}(x_D,0) - \frac{\partial \overline{T}_{f3D}}{\partial x_D} - \left.\frac{\partial \overline{T}_{m3D}}{\partial z_D}\right|_{z_D=0} = 0. \tag{B2}$$

Similar to (A14), the following is satisfied for $\overline{T}_{m3D}$:

$$\left.\frac{\partial \overline{T}_{m3D}}{\partial z_D}\right|_{z_D=0} = \left.\frac{\partial \overline{T}_{m3D,1}}{\partial z_D}\right|_{z_D=0} - \sqrt{s\theta}\,\overline{g}_3(x_D,s). \tag{B3}$$

Substituting (B3) for (B2), (B2) becomes

$$(s+\sqrt{s\theta})\overline{T}_{f3D} - h_3(x_D) - \frac{\partial \overline{T}_{f3D}}{\partial x_D} - \left.\frac{\partial \overline{T}_{m3D,1}}{\partial z_D}\right|_{z_D=0} = 0. \tag{B4}$$

Here the method of images is applied to extend the problem domain to $x_D = -\infty$. The initial condition $h_3(x_D)$ is assumed to be the even function. Applying the Fourier transform to (B4) with respect to x_D,

$$(s+\sqrt{s\theta})\hat{\overline{T}}_{f3D} - \hat{h}_3(\omega) - i\omega\hat{\overline{T}}_{f3D} - \left.\frac{\partial \hat{\overline{T}}_{m3D,1}}{\partial z_D}\right|_{z_D=0} = 0. \tag{B5}$$

Then,

$$\hat{\overline{T}}_{f3D} = \frac{1}{s+\sqrt{s\theta}-i\omega}\left[\hat{h}_3(\omega) + \left.\frac{\partial \hat{\overline{T}}_{m3D,1}}{\partial z_D}\right|_{z_D=0}\right]. \tag{B6}$$

By applying the inverse Fourier transform and using the Fourier convolution principle, the solution is obtained and re-expressed over the actual domain, $0 < x_D < \infty$.

$$\begin{aligned} \overline{T}_{f3D} = {} & U(-x_D)e^{(s+\sqrt{s\theta})x_D} * \left[h_3(x_D) + \left.\frac{\partial \overline{T}_{m3D,1}}{\partial z_D}\right|_{z_D=0}\right] \\ = {} & \int_{-\infty}^{\infty} U(-\xi)e^{(s+\sqrt{s\theta})\xi}\left[h_3(x_D-\xi) + \left.\frac{\partial \overline{T}_{m3D,1}(x_D-\xi,z_D,s)}{\partial z_D}\right|_{z_D=0}\right]\mathrm{d}\xi \\ = {} & \int_0^{\infty} e^{-(s+\sqrt{s\theta})\xi}\left[h_3(x_D+\xi) + \left.\frac{\partial \overline{T}_{m3D,1}(x_D+\xi,z_D,s)}{\partial z_D}\right|_{z_D=0}\right]\mathrm{d}\xi. \end{aligned} \tag{B7}$$

The inverse Laplace transform of (B7) with respect to s is

$$T_{f3D} = \int_0^{t_{3D}} \frac{\sqrt{\theta}\xi}{2} \frac{e^{-\theta\xi^2/4(t_{3D}-\xi)}}{\sqrt{\pi(t_{3D}-\xi)^3}} \times h_3(x_D+\xi)\,\mathrm{d}\xi + \int_0^{t_{3D}} \int_0^{\tau} \frac{\sqrt{\theta}\xi}{2} \frac{e^{-\theta\xi^2/4(\tau-\xi)}}{\sqrt{\pi(\tau-\xi)^3}} \times \left.\frac{\partial T_{m3D,1}}{\partial z_D}\right|_{z_D=0} \mathrm{d}\xi\,\mathrm{d}\tau. \quad \text{(B8)}$$

Similar to (A18),

$$\left.\frac{\partial T_{m3D,1}}{\partial z_D}\right|_{z_D=0} = \frac{\sqrt{\theta}}{2\sqrt{\pi t_{3D}}} \int_0^{\infty} f_3(x_D,\eta) \frac{\theta\eta}{t_{3D}} e^{-\theta\eta^2/4t_{3D}}\,\mathrm{d}\eta. \quad \text{(B9)}$$

Therefore, substituting (B9) and the initial condition (13) into (B8) yields the solution for the fracture temperature in the real domain during the withdrawal phase:

$$T_{f3D}(x_D,t_{3D}) = \int_0^{\min(t_{3D},t_{Dq}-x_D)} \frac{\sqrt{\theta}\xi}{2} \frac{e^{-\theta\xi^2/4(t_{3D}-\xi)}}{\sqrt{\pi(t_{3D}-\xi)^3}} \times T_{f3D}(x_D+\xi,0)\,\mathrm{d}\xi + \int_0^{t_{3D}} \int_0^{\min(\tau,t_{Dq}-x_D)} \frac{\sqrt{\theta}\xi}{2} \frac{e^{-\theta\xi^2/4(\tau-\xi)}}{\sqrt{\pi(\tau-\xi)^3}} \times \theta \int_0^{\infty} T_{m3D}(x_D+\xi,\eta,0) \times \frac{\sqrt{\theta}\eta}{2} \times \frac{e^{-\theta\eta^2/4(t_{3D}-\tau)}}{\sqrt{\pi(t_{3D}-\tau)^3}} \mathrm{d}\eta\,\mathrm{d}\xi\,\mathrm{d}\tau. \quad \text{(B10)}$$

Notation

Nomenclature

b half fracture aperture, m
c_f average specific heat of rock and fluid in fracture, J/kg/°C
c_m specific heat of rock matrix, J/kg/°C
c_w specific heat of water, J/kg/°C
k_m thermal conductivity of rock matrix, W/m/°C
H fracture height, m
p Laplace transform variable with respect to x
q volumetric flow rate, $m^3\ s^{-1}$
s Laplace transform variable with respect to t
t time (s)
t_i total injection time (s)
t_q total quiescent time (s)
t_s tracer injection time (s)
T temperature (°C)
T_{inj} temperature of injected fluid (°C)
T_0 initial reservoir temperature (°C)
v pore velocity ($m\ s^{-1}$)
x distance along flow direction (m)
z distance normal to flow direction (m)
ϕ_f porosity of fracture
ρ_f average density of rock and fluid in fracture (Kg/m^3)
ρ_m density of rock matrix (Kg/m^3)
ρ_w density of water (Kg/m^3)
θ dimensionless parameter in (3c) ($\theta = \rho_m c_m/\rho_f c_f$)
ω Fourier transform variable

Subscripts

f fracture
m matrix
w water
D dimensionless
1 injection phase
2 quiescent period
3 withdrawal phase

[46] **Acknowledgments.** This work was supported by the Assistant Secretary for Energy Efficiency and Renewable Energy, Office of Technology Development, Geothermal Technologies Program, of the U.S. Department of Energy under contract DE-AC02-05CH11231. The authors would like to thank C. Doughty for her careful review.

References

Doughty, C., and C.-F. Tsang (2009), Analysis of three sets of SWIW tracer test data using a two-population complex fracture model for diffusion and sorption, *Rep. LBNL-3006E*, Lawrence Berkeley Natl. Lab., Berkeley, Calif.

Folland, G. B. (1995), *Introduction to Partial Differential Equations*, 324 pp., Princeton Univ. Press, Princeton, N. J.

Gérard, A., A. Genter, T. Kohl, P. Lutz, P. Rose, and F. Rummel (2006), The Deep EGS (Enhanced Geothermal System) project at Soultz-sous-Forêts (Alsace, France), *Geothermics*, *35*(5–6), 473–483.

Ghergut, I., C. M. Dermott, M. Sauter, M. Herfort, and O. Kolditz (2006), Reducing ambiguity in fractured-porous media characterization using single-well tracer tests, in *ModelCARE-2005: From Uncertainty to Decision Making*, edited by K. Kovar et al., pp. 17–24, IAHS Red Book 304, Wallingford, U. K.

Ghergut, I., M. Sauter, H. Behrens, T. Licha, T. Tischner, and R. Jung (2009), Single-well dual-tracer spikings during EGS creation in Northern German sedimentary layers, paper presented at Thirty-Fourth Workshop on Geothermal Reservoir Engineering, Stanford Univ., Stanford, Calif.

Haggerty, R., S. W. Fleming, L. C. Meigs, and S. A. McKenna (2001), tracer tests in a fractured dolomite, 2. Analysis of mass transfer in single-well injection-withdrawal tests, *Water Resour. Res.*, *37*(5), 1129–1142.

Hellström, G., and C.-F. Tsang (1988a), Buoyancy flow at a two-fluid interface in a porous medium: Analytical studies, *Water Resour. Res*, *24*(4), 493–506.

Hellström, G., and C.-F. Tsang (1988b), Combined forced-convection and buoyancy flow at a two-fluid interface in a porous medium: Analytical studies, *Water Resour. Res.*, *24*(4), 507–515.

Kocabas, I. (2005), Geothermal reservoir characterization via thermal injection backflow and interwell tracer testing, *Geothermics*, *34*, 27–46.

Kocabas, I. (2010), Designing thermal and tracer injection backflow tests, paper presented at World Geothermal Congress 2010, Bali, Indonesia.

Kocabas, I., and R. N. Horne (1987), Analysis of injection-backflow tracer tests in fractured geothermal reservoirs, paper presented at Twelfth Workshop on Geothermal Reservoir Engineering, Stanford Univ., Stanford, Calif.

Kocabas, I., and R. N. Horne (1990), A new method of forecasting the thermal breakthrough time during reinjection in geothermal reservoirs, paper presented at Fifteenth Workshop on Geothermal Reservoir Engineering, Stanford Univ., Stanford, Calif.

Lauwerier, H. A. (1955), The transport of heat in an oil layer caused by the injection of hot fluid, *Appl. Sci. Res.*, *5*(2–3), 145–150.

Moreno, L., B. Gylling, and I. Neretnieks (1997), Solute transport in fractured media—the important mechanisms for performance assessment, *J. Contam. Hydr.*, *25*, 283–298.

Nalla, G., and G. M. Shook (2005), Novel application of single-well tracer tests to evaluate hydraulic stimulation effectiveness, *GRC Trans.*, *29*, 177–181.

Neretnieks, I. (2007), Single well injection withdrawal tests (SWIW) in fractured rock—some aspects on interpretation, *Rep. R-07-54*, Dep. of Chem. Eng. and Technol., Royal Inst. of Tech., Stockholm, Sweden.

Neretnieks, I., and L. Moreno (2003), Prediction of some in situ tracer tests with sorbing tracers using independent data, *J. Contam. Hydr.*, *61*, 351–360.

Pruess, K. (2002), Numerical simulation of multiphase tracer transport in fractured geothermal reservoirs, *Geothermics*, *31*, 475–499.

Pruess, K., and C. Doughty (2010), Thermal single-well injection-withdrawal tracer tests for determining fracture-matrix heat transfer area, paper presented at Thirty-Fifth Workshop on Geothermal Reservoir Engineering, Stanford Univ., Stanford, Calif.

Pruess, K., C. Oldenburg, and G. Moridis (1999), *TOUGH2 User's Guide, Version 2.0, Rep. LBNL-43134*, Lawrence Berkeley Natl. Lab., Berkeley, Calif.

Pruess, K., T. van Heel, and C. Shan (2005), Tracer testing for estimating heat transfer area in fractured reservoirs, paper presented at World Geothermal Congress 2005, Antalya, Turkey.

Sanjuan, B., J.-L. Pinault, P. Rose, A. Gérard, M. Brach, G. Braibant, C. Crouzet, J.-C. Foucher, A. Gautier, and S. Touzelet (2006), Tracer testing of the geothermal heat exchanger at Soultz-sous-Forêts (France) between 2000 and 2005, *Geothermics*, *35*(5–6), 622–653.

Schroth, M. H., J. D. Istok, and R. Haggerty (2001), In situ evaluation of solute retardation using single-well push-pull test, *Adv. Water Resour.*, *24*, 105–117.

Shan, C., and K. Pruess (2005), An analytical solution for slug tracer tests in fractured reservoirs, *Water Resour. Res.*, *41*, W08502, doi:10.1029/2005WR004081.

Shook, G. M. (2001), Predicting thermal breakthrough in heterogeneous media from tracer tests, *Geothermics*, *30*(6), 573–589.

Y. Jung and K. Pruess, Earth Science Division, Lawrence Berkeley National Laboratory, 1 Cyclotron Rd., MS 90-1116, Berkeley, CA 94720, USA. (yoojinjung@lbl.gov)